Dirac fermions in the layered titanium-based oxypnictide superconductor $BaTi_2Bi_2O$

Xianbiao Shi,[1,2] Li Chen,[4] Peng He,[1,2,*] Guangtao Wang,[5] Gongping Zheng,[5] Xin Liu,[4,†] and Weiwei Zhao[1,2,3,‡]

[1]*State Key Laboratory of Advanced Welding and Joining, Harbin Institute of Technology, Shenzhen 518055, People's Republic of China*

[2]*Flexible Printed Electronics Technology Center, Harbin Institute of Technology, Shenzhen 518055, People's Republic of China*

[3]*Key Laboratory of Micro-systems and Micro-structures Manufacturing of Ministry of Education, Harbin Institute of Technology, Harbin 150001, People's Republic of China*

[4]*School of Physics and Wuhan National High Magnetic Field Center, Huazhong University of Science and Technology, Wuhan, Hubei 430074, People's Republic of China*

[5]*College of Physics and Materials Science, Henan Normal University, Xinxiang 453007, People's Republic of China*

(Received 13 August 2018; revised manuscript received 10 April 2019; published 30 April 2019)

First-principles calculations and effective model analysis are used to prove the existence of a single pair of three-dimensional Dirac points in the well-known layered titanium-based oxypnictide superconductor $BaTi_2Bi_2O$. The nontrivial topological character of $BaTi_2Bi_2O$ is demonstrated by calculating the surface states. The Dirac points, residing on the rotational axis, are found approximately 70 meV below the Fermi level which can be lifted to Fermi surface by Sb doping. The Dirac points and related physics are expected to be detected by angle-resolved photoemission spectroscopy. This compound is also found to be a superconductor with transition temperature (T_c) 4.6 K; our results may provide an appropriate platform to study the interplay between topological Dirac fermions and superconductivity.

DOI: 10.1103/PhysRevB.99.155155

I. INTRODUCTION

The materials that host band crossing points near the Fermi level (E_f), namely, topological semimetals (TSMs), are currently undergoing intense scrutiny [1–3]. Depending on band degeneracy and the momentum space distribution of the band-crossing points, three different types of TSMs, say Dirac semimetal (DSM) [4–7], Weyl semimetal (WSM) [8–11], and nodal-line semimetal (NLSM) [12–15], have been proposed. DSM is the three-dimensional (3D) analog of graphene whose quasiparticle excitations are described by massless Dirac fermions. DSMs have been theoretically predicted and experimentally observed in Na_3Bi [4,5] and Cd_3As_2 [6,7] with many interesting properties, such as high carrier mobility, chiral anomaly induced negative magnetoresistivity (MR), Shubnikov–de Haas (SdH) oscillation, and unique surface states [1–3].

The nontrivial topological surface states have been proposed to obtain quasiparticle excitations, particularly Majorana fermions [16–18], which are of great potential interest for topological quantum computation [19]. To obtain Majorana fermions, the scenarios based on either the p-wave superconductor or the heterostructure between topological material and s-wave superconductor were constructed. A p-wave superconductor can be an intrinsic topological superconductor [20–23], including Sr_2RuO_4 [24,25] and $Cu_xBi_2Se_3$ [26,27] as the promising candidates. The proximity effect could induce superconductivity in the topological surface states, resulting an equivalent spinless $p_x + ip_y$ type superconductor [17,28]. The reported p-wave superconductor candidates remain scarce meanwhile the topological insulator – superconductor heterostructures are very complicated. These make the exploration and application of Majorana fermions very challenging. Thus it is worth searching for topological superconductors in new materials.

The coexistence of superconductivity and topological band structure has been theoretically predicted [29–31] and experimentally confirmed [29,32] on the surface of iron-based superconductor (IBSC) $FeTe_{0.55}Se_{0.45}$. This provides a route to design and discover topological superconductors. Exploring the layered materials that integrate nontrivial band topology with s-wave bulk superconductivity is a more promising approach to engineer topological superconductors. We focus on titanium-based oxypnictide superconductor (TBSC) [33–36]. The TBSC shares a number of common features with the IBSC, as it is a layered structure containing square planes of transition element atoms, Ti. The coherence length of the TBSC [36] is longer than $FeTe_{1-x}Se_x$ [37]. The superconducting symmetry of the TBSC has been classified as an ordinary s-wave state based on the nuclear magnetic resonance/nuclear quadrupole resonance measurements [38].

We use first-principles calculations to predict that the well-known superconductor $BaTi_2Bi_2O$ is a topological superconductor candidate. We show that $BaTi_2Bi_2O$ can host a pair of symmetry protected Dirac points along the k_z axis. The Dirac points originate from a band inversion at Γ point. Similar to prominent DSMs, Na_3Bi [4,5] and Cd_3As_2 [6,7], topologically nontrivial surface states near the E_f can be clearly observed on the (010) projected surface.

II. METHOD AND CRYSTAL STRUCTURE

The structural relaxation and electronic structure calculation were performed by employing the density functional

*hithepeng@hit.edu.cn
†phyliuxin@hust.edu.cn
‡Corresponding author: wzhao@hit.edu.cn

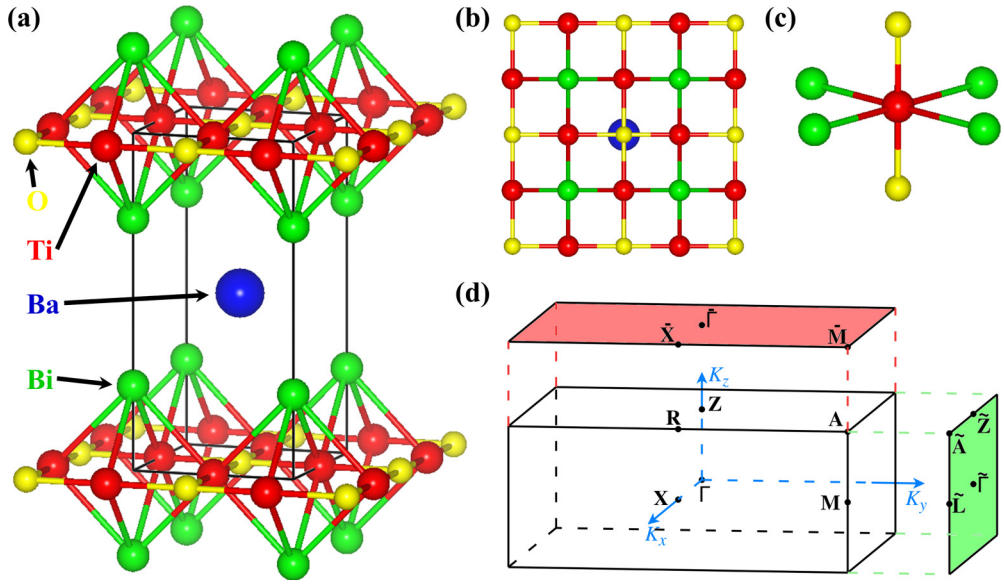

FIG. 1. (a) Crystal structure of $BaTi_2Bi_2O$ with a uniform stacking of $[Ti_2Bi_2O]$ layers along the tetragonal c axis. (b) View along the c axis. (c) Coordination geometry of the TiO_2Bi_4 octahedron. (d) The bulk BZ and the associated (001) and (010) projected surfaces BZ.

theory (DFT) that was encoded in the Vienna *ab inito* simulation package (VASP) [39–41] with the projector augmented wave (PAW) method [42,43]. The Perdew-Burke-Ernzerhof (PBE) [44] type generalized gradient approximation (GGA) [45] was adopted to include the exchange-correlation effects. The plane-wave energy cutoff was fixed to 500 eV and the Γ-centered k-point mesh of $12\times12\times6$ was used to sample the Brillouin zone (BZ). The energy and force difference criterion were defined as 10^{-6} eV and 0.01 eV/Å for self-consistent convergence and structural relaxation. The DFT results were used to construct Wannier functions [46,47] for Ba-5d, Ti-3d, Bi-6p, and O-2p atomic orbitals and determine the hopping parameter values for tight-binding model. The topological features of surface-state spectra were calculated using the iterative Green's-function technique [48], which was implemented in the WANNIER-TOOLS package [49].

$BaTi_2Bi_2O$ has been synthesized by conventional solid-state reaction method and shows superconductivity with $T_c = 4.6$ K [35]. This compound crystallizes in a tetragonal structure with space group $P/4mmm$ (no. 123) and has a layered structure, as shown in Fig. 1(a). This layered structure resembles the iron-based and cuprate superconductors. The Ti atom is twofold coordinated with O atoms, forming a planer square lattice of Ti_2O [Fig. 1(b)], which adopts the anticonfiguration of Cu_2O structure in the high-T_c cuprates. The Ti atom is also fourfold coordinated with Bi atoms, resulting in a Ti_2Bi_2O layer where the Bi atoms are placed above and below the center of the Ti square. The Ti atom is octahedrally coordinated by two O atoms and four Bi atoms [Fig. 1(c)]. The crystal is formed by stacking the Ti_2Bi_2O layers alternately with layers of Ba atoms along the c direction. This particular stacking preserves the space-inversion symmetry. We optimize the internal Bi height parameter z_{Bi} with the fixed lattice parameters to experimental values. We obtain $z_{Bi} = 0.7483$, which agree well with the experimental value ($z_{Bi} = 0.7487$) [35]. This is in contrast to the large underestimation from the DFT calculations found in the IBSCs [50,51]. The optimized Bi height is used in the electronic structure calculations. Figure 1(d) presents the bulk BZ, the associated (001), and (010) projected surfaces BZ.

III. RESULTS AND DISCUSSION

A. Electronic structures

Figure 2 presents the calculated total density of states (DOS) and the atomic species projected density of states (PDOS) of $BaTi_2Bi_2O$ with turning on spin-orbit coupling (SOC) effect. The total DOS without SOC effect is shown for comparison. The SOC does not have a large effect on the

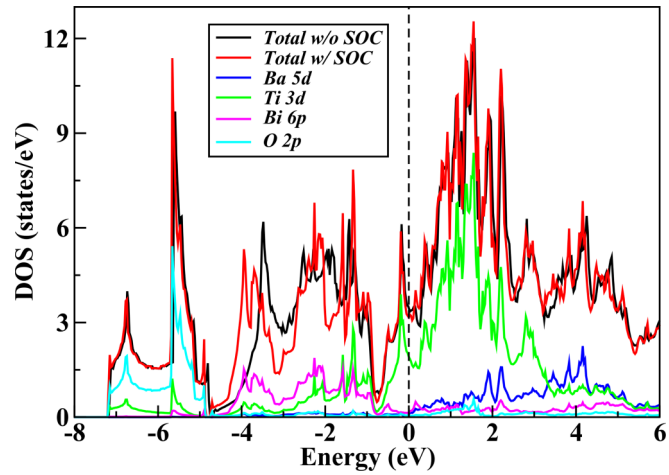

FIG. 2. The calculated total DOS and PDOS of $BaTi_2Bi_2O$. The total DOS calculated without and with considering SOC are shown in black and red lines. The presented PDOS are calculated with turning on SOC effect.

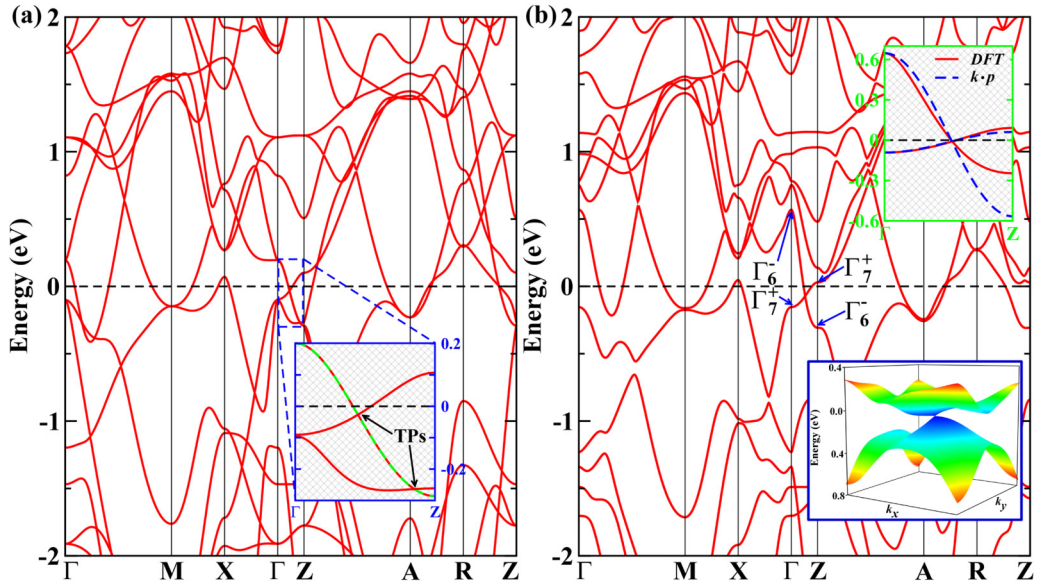

FIG. 3. (a) The energy band structure of $BaTi_2Bi_2O$ without turning on SOC effect. The inset shows a zoomed-in feature near the E_f along the Γ-Z direction, the arrows point out the energy band's triply degenerate points. (b) The energy-band structure of $BaTi_2Bi_2O$ with turning on SOC effect. Γ_6^- and Γ_7^+ indicate the irreducible representations and parity of the two crossing bands at high-symmetry point Γ and Z, respectively. The blue dashed lines in upper inset are the results from $k \cdot p$ model. The lower inset denotes 3D band structure of the corresponding Dirac cone.

DOS near the E_f. It does affect the DOS in the energy region from −4.2 eV to −1.5 eV. The DOS of $BaTi_2Bi_2O$ resembles the Ti_2Pn_2O (Pn = As or Sb) layer based systems [52–56], and exhibits typical characteristics of the layered structure. The PDOS shows that the states at the E_f are dominated by Ti-3d states. The Ti-3d localizes at the energy region (−0.8 ∼ 3.5) eV, and has considerable distributions between −4.0 and −0.8 eV, where Bi-6p states mostly locate, showing the sizable hybridization between Ti and Bi states. The O-2p derived states primarily lie −5 eV below the E_f. The Ba-5d derived states have a large unoccupied component above the E_f. The conduction in $BaTi_2Bi_2O$ primarily occurs in the Ti_2Bi_2O layers [57].

The Dirac point is illustrated via the band structure of $BaTi_2Bi_2O$; see Fig. 3. Without considering SOC [Fig. 3(a)], there are three bands crossing the E_f, implying the multiorbital nature superconductivity in $BaTi_2Bi_2O$ [58]. There are two band crossing points located along the Γ-Z line. We then focus on the band structure along the Γ-Z line. The zoom in of band structure along the Γ-Z line [inset of Fig. 3(a)] shows the doubly degenerate bands (green solid and red dashed curves) which connect the conduction at Γ and the valence at Z. Along the Γ-Z line, the degenerate bands display strongly downward dispersion. The inset of Fig. 3(a) also shows another two nondegenerated bands (red solid curves). One connects the valence at Γ and the conduction at Z, and the other connects the valence at both Γ and Z. As a result, there are two band crossing points among them which are thus triple points (TPs), triply degenerate, indicated by arrows in the inset of Fig. 3(a). According to Ref. [59]'s definition, the TPs in $BaTi_2Bi_2O$ belong to type A, as the Berry phase around the Γ-Z line is zero. The topology induced surface states of TPs would only appear in a system with SOC, and would not emerge in the absence of SOC case [60].

When SOC is considered, the band structure near the E_f along the Γ-Z line dramatically changed. As plotted in Fig. 3(b), there is a linear band crossing near the E_f between Γ and Z. The band crossing point is located at the BZ coordinate (0, 0, $k_z^D \approx \pm 0.26 \times \frac{\pi}{c}$) and energy E_{DPs}-$E_f \approx$ −70 meV. The two relevant bands are both doubly degenerate attributed to time-reversal and space-inversion symmetries in $BaTi_2Bi_2O$. The band crossing point is actually fourfold degenerate, namely the Dirac point. At the Γ point, the lowest unoccupied band and the highest occupied band belong to Γ_6 and Γ_7 irreducible representations of the D_{4h} double group, and with different parties. At the Z point, these two bands exchange their order [Fig. 3(b)], indicating an inverted band structure. The band inversion leads to the nontrivial band topology for $BaTi_2Bi_2O$. The little group is C_{4v} for any k point along the Γ-Z line. The two inverted bands are Λ_6 and Λ_7 irreducible representations of the C_{4v} double group. The different representation prohibits the hybridization between them, resulting in the protected band crossing [6]. The Dirac node in the Γ-Z line is unavoidable. It is protected by the C_4 rotational symmetry. In the lower inset of Fig. 3(b), a 3D plot of the highest valence and the lowest conduction bands is presented, where the Dirac point is clearly observed.

B. Topological surface states

The nontrivial bulk band topology of 3D DSM is expected to result in topological surface states on the surface. In order to further confirm the topological character of $BaTi_2Bi_2O$, we calculated the surface states on both (001) and (010) surfaces whose BZs are perpendicular and parallel to the Γ-Z direction. Figures 4(a) and 4(b) illustrate the surface states and bulk bands projected onto the (001) surface. On this surface,

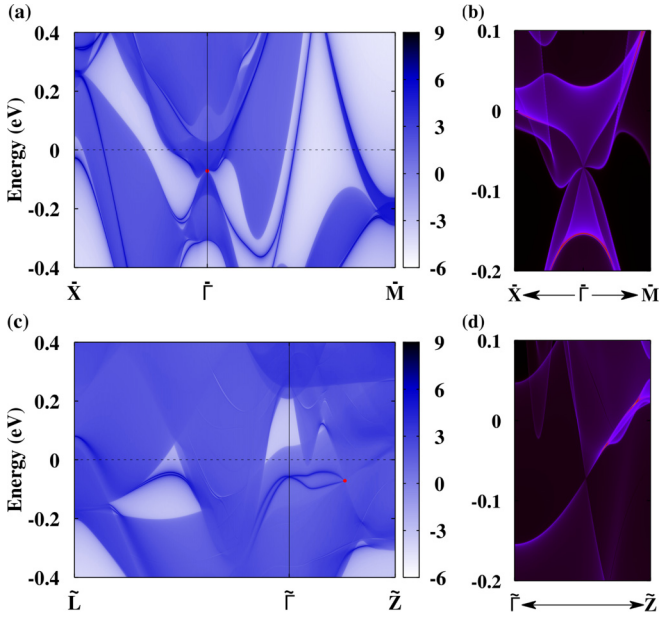

FIG. 4. (a) Projected surface states for the (001) surface of $BaTi_2Bi_2O$. The red dot labels the projected Dirac point. (b) Projected bulk bands onto (001) surface. (c), (d) Identical to (a) and (b) but for the (010) surface.

the pair of bulk Dirac points distributed on the k_z axis are projected onto the same surface $\bar{\Gamma}$ point, which is labeled by the red dot in Fig. 4(a). Since the bands are inverted at Γ point in the bulk, the expected Dirac cone type surface states that are similar to topological insulator case are seen. Figure 4(b) shows that the gapless linear dispersion bulk states are observed. For the (010) surface, the electronic spectrum is different. This side surface is parallel to the k_z axis, so the two bulk Dirac points are projected to different points. As shown in Fig. 4(c), the nontrivial surface states that emerge from the Dirac points and merge in bulk states are clearly visible, which is a direct evidence for nontrivial topology.

There is a topological surface Dirac cone at the $\tilde{\Gamma}$ point [Fig. 4(c)], and it separates from the projection of the bulk Dirac cone [Fig. 4(d)]. The bulk Dirac points and the surface Dirac cone are 70 meV below the E_f, and could be observed by ARPES. In Fig. 5(a), we show that the position of bulk Dirac points can be tuned to the E_f by Sb doping. The Dirac points can be lifted to the E_f by means of Sb substitution with 0.4%. Meanwhile, the superconducting transition temperature of $BaTi_2Bi_2O$ decreases very slightly during Sb doping [58]. Thus the surface electrons in this Dirac cone could have superconductivity due to the proximity effect of the bulk superconductivity, making $BaTi_2Bi_2O$ a candidate for a topological superconductor. According to Ref. [17]'s proposal, each vortex of topological superconductors has a Majorana zero mode. Compared to other topological superconductor candidates, Sr_2RuO_4 ($T_c = 0.93$ K) [24], Au_2Pb ($T_c = 1.2$ K) [61], $PdTe_2$ ($T_c = 1.64$ K) [62], $Cu_xBi_2Se_3$ ($T_c = 3.8$ K) [26], and $PbTaSe_2$ ($T_c = 3.8$ K) [63], $BaTi_2Bi_2O$ possesses a higher superconducting transition temperature of 4.6 K.

C. Effective $k \cdot p$ model

To further understand the low-energy Dirac fermions and discuss the proximity induced superconductivity in the surface states, we construct the $k \cdot p$ effective model around the Dirac points, based on the symmetry constraints. We first consider the case without SOC. The first-principles calculations indicate that the wave functions of low-energy states at the Γ point are mostly from Bi-p_z, Ba-$d_{x^2-y^2}$, and Bi-p_x, p_y states. As shown in Fig. 1(a), the unit cell contains one Ba atom and two Bi atoms. We can construct the above relevant orbitals from bonding and antibonding states as

$$|P_\alpha^-\rangle = \frac{1}{\sqrt{2}}(|\mathrm{Bi}, p_\alpha\rangle + |\mathrm{Bi}', p_\alpha\rangle),$$
$$|D_{x^2-y^2}^+\rangle = |\mathrm{Ba}, d_{x^2-y^2}\rangle, \quad (1)$$

where Bi and Bi$'$ are related by inversion with $\alpha = x, y, z$. The superscript $+(-)$ on the left-hand side of Eq. (1) indicates the even (odd) parity.

When including the SOC effect, we find that there is a band crossing between two doubly degenerate states in the Γ-Z direction which leads to a topological nontrivial band structure. According to the orbital component analysis of the wave function at the Γ point, the main components of the two doubly degenerate states are $\left|D_{\frac{5}{2}}^+, \pm\frac{5}{2}\right\rangle$ and $\left|P_{\frac{3}{2}}^-, \pm\frac{1}{2}\right\rangle$ which belong to Γ_7^+ and Γ_6^- representations, respectively, where the subscript

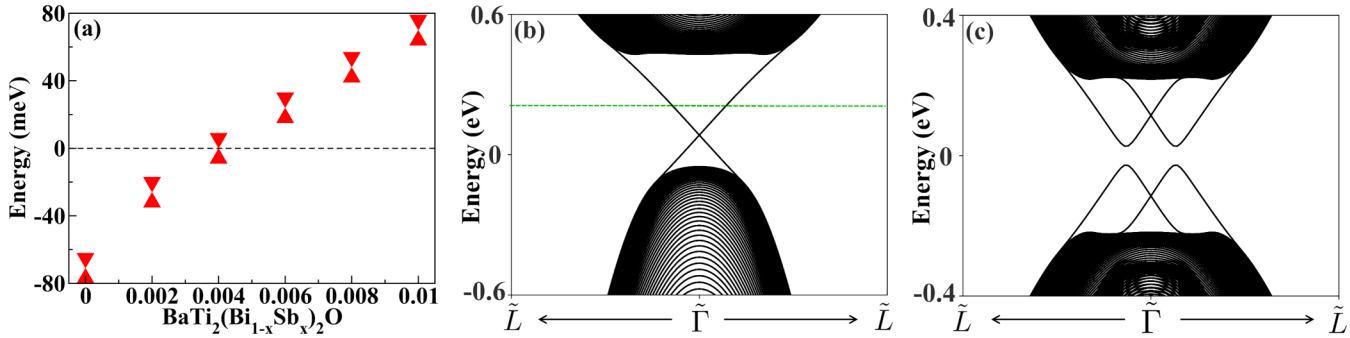

FIG. 5. (a) Variations of the position of bulk Dirac points with Sb content x for $BaTi_2(Bi_{1-x}Sb_x)_2O$. The results are obtained from the virtual crystal approximation (VCA) which indicates that 0.4% doping will put Dirac points precisely on the E_f. (b) The (010) surface states near the $\tilde{\Gamma}$ point of 0.4% Sb doped $BaTi_2Bi_2O$. (c) The superconducting (010) surface states with finite chemical potential represented by the green dashed line in (b).

indicates the total angular momentum J. We use these four states (in the order of $|D^+_{5/2}, \frac{5}{2}\rangle$, $|D^+_{5/2}, -\frac{5}{2}\rangle$, $|P^-_{3/2}, \frac{1}{2}\rangle$, and $|P^-_{3/2}, -\frac{1}{2}\rangle$) as bases to construct a four-band $k \cdot p$ effective model.

The point group of $BaTi_2Bi_2O$ at the Γ point with a spin internal degree of freedom is the D_{4h} double group. The three generators of D_{4h} include spatial inversion $\widehat{I}$, fourfold rotation $\widehat{C}_{4z}$, and twofold rotation $\widehat{C}_{2y}$. The representations of group generators together with time-reversal operator $\widehat{T}$ according to the bases are given by

$$\widehat{C}_{4z} = \begin{pmatrix} e^{i3\pi/4} & 0 & 0 & 0 \\ 0 & e^{-i3\pi/4} & 0 & 0 \\ 0 & 0 & e^{-i\pi/4} & 0 \\ 0 & 0 & 0 & e^{i\pi/4} \end{pmatrix}, \tag{2}$$

$$\widehat{C}_{2y} = \begin{pmatrix} 0 & -1 & 0 & 0 \\ 1 & 0 & 0 & 0 \\ 0 & 0 & 0 & 1 \\ 0 & 0 & -1 & 0 \end{pmatrix}, \quad \widehat{I} = \begin{pmatrix} 1 & 0 & 0 & 0 \\ 0 & 1 & 0 & 0 \\ 0 & 0 & -1 & 0 \\ 0 & 0 & 0 & -1 \end{pmatrix}, \tag{3}$$

$$\widehat{T} = \begin{pmatrix} 0 & -1 & 0 & 0 \\ 1 & 0 & 0 & 0 \\ 0 & 0 & 0 & 1 \\ 0 & 0 & -1 & 0 \end{pmatrix} K, \tag{4}$$

where K is the complex conjugation operator. The $k \cdot p$ Hamiltonian is obtained by the constraint

$$D(R)H(k)D(R)^\dagger = H[R(k)], \tag{5}$$

where $D(R)$ is the representative matrix of the symmetry operator R mentioned above. A four-band model up to the second order of k around the Γ point is given by

$$H_0(\boldsymbol{k}) = \begin{pmatrix} M_1(\boldsymbol{k}) & 0 & 0 & \beta k_- \\ 0 & M_1(\boldsymbol{k}) & -\beta k_+ & 0 \\ 0 & -\beta k_- & M_2(\boldsymbol{k}) & 0 \\ \beta k_+ & 0 & 0 & M_2(\boldsymbol{k}) \end{pmatrix}, \tag{6}$$

$$M_n(\boldsymbol{k}) = E_n + \frac{k_x^2 + k_y^2}{2m_{nx}} + t_{nz}[1 - \cos(ck_z)], \tag{7}$$

where $n = 1, 2$ indicates the orbitals with E_n (the eigenenergy of the band n at the Γ point), m_{nx} and t_{nz} are the in-plane effective mass and the z direction hopping of band n, and β is the interband hopping strength, $k_\pm = k_x \pm ik_y$. In order to describe the band dispersion along the Γ-Z direction well, this Hamiltonian is written as a combination of an in-plane $k \cdot p$ model and a z direction tight-binding model. By fitting the energy spectrum of the effective Hamiltonian with DFT calculations in the Γ-Z direction, the parameters are determined as $E_1 = -0.092$ eV, $E_2 = 0.647$ eV, $t_{1z} = 0.075$ eV, and $t_{2z} = -0.605$ eV. The fitting curves (blue dashed lines) reproduce the band crossing point of the DFT calculations (red lines), as shown in the upper inset of Fig. 3(b). The $k \cdot p$ curves match well with the DFT calculations around the Dirac point but deviate gradually from DFT calculated band for the momentum away from the Dirac point. This is because in $k \cdot p$ calculations, we only consider the two doubly degenerate bands near the E_f and neglect their coupling with other bands which however will not affect the topology of the bands.

Using the effective Hamiltonian H_0, we investigate the (010) surface states by considering a thick slab limited in $y \in [-d/2, d/2]$ with d the thickness of the slab. The Hamiltonian for the slab structure can be obtained by Fourier transformation of $H_0(k_x, k_z, k_y)$ to $H_0(kx, kz, -i\partial_y)$. To avoid possible confusion of bulk and surface gapless dispersion, we further choose $k_z = 0$, which is away from the bulk Dirac point, so that the gapless dispersion shown in Fig. 5(b) is clearly from surface states.

When introducing a conventional s-wave superconducting pairing, the BdG Hamiltonian of the system is

$$H_{\mathrm{BdG}}(\boldsymbol{k}) = \begin{pmatrix} H_0(\boldsymbol{k}) - \mu & \Delta i\sigma_0 s_y \\ -\Delta i\sigma_0 s_y & -H_0^*(-\boldsymbol{k}) + \mu \end{pmatrix}, \tag{8}$$

where μ is the chemical potential, Δ is the pairing amplitude, and $\boldsymbol{\sigma}$ and $\boldsymbol{s}$ are Pauli matrices acting on the orbital and spin space, respectively. With finite chemical potential μ, we note that the surface states are gapped by superconductivity [see Fig. 5(c)].

IV. SUMMARY

In summary, at first we present electronic structure calculations of a layered superconductor $BaTi_2Bi_2O$ which hosts a pair of Dirac points. The Dirac points are derived from band inversion and protected by C_4 crystal symmetry. The nontrivial surface states are obtained on both (001) and (010) surfaces. Then we construct an effective $k \cdot p$ model and reproduce the band dispersion in the Γ-Z direction with DFT calculations. According to the effective model, we obtain the surface states near the $\tilde{\Gamma}$ point which are consistent with the DFT calculations. When superconductivity is introduced, the surface states are gapped which can be a candidate for topological superconductor. Although the Dirac point is well below the E_f according to our DFT calculations, we note that by 0.4% Sb doping, the Dirac point can be shifted near the E_f which is expected to be observed in experiments.

ACKNOWLEDGMENTS

This work was supported by Shenzhen Science and Technology Innovation Committee (Grant No. JCYJ20170811160129498), Open Research Fund Program of the State Key Laboratory of Low-Dimensional Quantum Physics (Grant No. KF201701), Key Laboratory of Micro-systems and Micro-structures Manufacturing of Ministry of Education, Harbin Institute of Technology (Grant No. 2017KM001), and Science and Technology Innovation Talents Program of Henan Province (Grant No. 174200510010). This work was also supported by the High Performance Computing Center of Henan Normal University.

X.S. and L.C. contributed equally to this work.

[1] H. M. Weng, X. Dai, and Z. Fang, J. Phys.: Condens. Matter **28**, 303001 (2016).
[2] B. A. Bernevig, H. M. Weng, Z. Fang, and X. Dai, J. Phys. Soc. Jpn. **87**, 041001 (2018).
[3] M. Hirayama, R. Okugawa, and S. Murakami, J. Phys. Soc. Jpn. **87**, 041002 (2018).
[4] Z. Wang, Y. Sun, X.-Q. Chen, C. Franchini, G. Xu, H. Weng, X. Dai, and Z. Fang, Phys. Rev. B **85**, 195320 (2012).
[5] Z. K. Liu, B. Zhou, Y. Zhang, Z. J. Wang, H. M. Weng, D. Prabhakaran, S.-K. Mo, Z. X. Shen, Z. Fang, X. Dai, Z. Hussain, and Y. L. Chen, Science **343**, 864 (2014).
[6] Z. Wang, H. Weng, Q. Wu, X. Dai, and Z. Fang, Phys. Rev. B **88**, 125427 (2013).
[7] Z. K. Liu, J. Jiang, B. Zhou, Z. J. Wang, Y. Zhang, H. M. Weng, D. Prabhakaran, S.-K. Mo, H. Peng, P. Dudin, T. Kim, M. Hoesch, Z. Fang, X. Dai, Z. X. Shen, D. L. Feng, Z. Hussain, and Y. L. Chen, Nat. Mater. **13**, 677 (2014).
[8] X. Wan, A. M. Turner, A. Vishwanath, and S. Y. Savrasov, Phys. Rev. B **83**, 205101 (2011).
[9] G. Xu, H. M. Weng, Z. J. Wang, X. Dai, and Z. Fang, Phys. Rev. Lett. **107**, 186806 (2011).
[10] H. Weng, C. Fang, Z. Fang, B. A. Bernevig, and X. Dai, Phys. Rev. X **5**, 011029 (2015).
[11] S.-M. Huang, S.-Y. Xu, I. Belopolski, C.-C. Lee, G. Chang, B. Wang, N. Alidoust, G. Bian, M. Neupane, C. Zhang, S. Jia, A. Bansil, H. Lin, and M. Z. Hasan, Nat. Commun. **6**, 7373 (2015).
[12] G. P. Mikitik and Y. V. Sharlai, Phys. Rev. B **73**, 235112 (2006).
[13] A. A. Burkov, M. D. Hook, and L. Balents, Phys. Rev. B **84**, 235126 (2011).
[14] M. Phillips and V. Aji, Phys. Rev. B **90**, 115111 (2014).
[15] R. Yu, H. Weng, Z. Fang, X. Dai, and X. Hu, Phys. Rev. Lett. **115**, 036807 (2015).
[16] X. L. Qi and S. C. Zhang, Rev. Mod. Phys. **83**, 1057 (2011).
[17] L. Fu and C. L. Kane, Phys. Rev. Lett. **100**, 096407 (2008).
[18] F. Wilczek, Nat. Phys. **5**, 614 (2009).
[19] S. R. Elliott and M. Franz, Rev. Mod. Phys. **87**, 137 (2015).
[20] N. Read and D. Green, Phys. Rev. B **61**, 10267 (2000).
[21] D. A. Ivanov, Phys. Rev. Lett. **86**, 268 (2001).
[22] A. Stern, F. von Oppen, and E. Mariani, Phys. Rev. B **70**, 205338 (2004).
[23] M. Stone and S. B. Chung, Phys. Rev. B **73**, 014505 (2006).
[24] Y. Maeno, H. Hashimoto, K. Yoshida, S. Nishizaki, T. Fujita, J. G. Bednorz, and F. Lichtenberg, Nature (London) **372**, 532 (1994).
[25] S. Das Sarma, C. Nayak, and S. Tewari, Phys. Rev. B **73**, 220502(R) (2006).
[26] Y. S. Hor, A. J. Williams, J. G. Checkelsky, P. Roushan, J. Seo, Q. Xu, H. W. Zandbergen, A. Yazdani, N. P. Ong, and R. J. Cava, Phys. Rev. Lett. **104**, 057001 (2010).
[27] L. A. Wray, S.-Y. Xu, Y. Xia, Y. S. Hor, D. Qian, A. V. Fedorov, H. Lin, A. Bansil, R. J. Cava, and M. Z. Hasan, Nat. Phys. **6**, 855 (2010).
[28] H.-H. Sun, K.-W. Zhang, L.-H. Hu, C. Li, G.-Y. Wang, H.-Y. Ma, Z.-A. Xu, C.-L. Gao, D.-D. Guan, Y.-Y. Li, C. Liu, D. Qian, Y. Zhou, L. Fu, S.-C. Li, F.-C. Zhang, and J.-F. Jia, Phys. Rev. Lett. **116**, 257003 (2016).
[29] Z. Wang, P. Zhang, G. Xu, L. K. Zeng, H. Miao, X. Xu, T. Qian, H. Weng, P. Richard, A. V. Fedorov, H. Ding, X. Dai, and Z. Fang, Phys. Rev. B **92**, 115119 (2015).
[30] X. X. Wu, S. S. Qin, Y. Liang, H. Fan, and J. P. Hu, Phys. Rev. B **93**, 115129 (2016).
[31] G. Xu, B. Lian, P. Z. Tang, X.-L. Qi, and S.-C. Zhang, Phys. Rev. Lett. **117**, 047001 (2016).
[32] P. Zhang, K. Yaji, T. Hashimoto, Y. Ota, T. Kondo, K. Okazaki, Z. Wang, J. Wen, G. D. Gu, H. Ding, and S. Shin, Science **360**, 182 (2018).
[33] P. Doan, M. Gooch, Z. Tang, B. Lorenz, A. Möller, J. Tapp, P. C. W. Chu, and A. M. Guloy, J. Am. Chem. Soc. **134**, 16520 (2012).
[34] T. Yajima, K. Nakano, F. Takeiri, T. Ono, Y. Hosokoshi, Y. Matsushita, J. Hester, Y. Kobayashi, and H. Kageyama, J. Phys. Soc. Jpn. **81**, 103706 (2012).
[35] T. Yajima, K. Nakano, F. Takeiri, J. Hester, T. Yamamoto, Y. Kobayashi, N. Tsuji, J. Kim, A. Fujiwara, and H. Kageyama, J. Phys. Soc. Jpn. **82**, 013703 (2013).
[36] T. Yajima, K. Nakano, Y. Nozaki, and H. Kageyama, Physica C (Amsterdam) **504**, 36 (2014).
[37] H. C. Lei, R. W. Hu, E. S. Choi, J. B. Warren, and C. Petrovic, Phys. Rev. B **81**, 094518 (2010).
[38] S. Kitagawa, K. Ishida, K. Nakano, T. Yajima, and H. Kageyama, Phys. Rev. B **87**, 060510(R) (2013).
[39] G. Kresse and J. Hafner, Phys. Rev. B **47**, 558 (1993).
[40] G. Kresse and J. Furthmüller, Comput. Mater. Sci. **6**, 15 (1996).
[41] G. Kresse and J. Furthmüller, Phys. Rev. B **54**, 11169 (1996).
[42] P. E. Blöchl, Phys. Rev. B **50**, 17953 (1994).
[43] J. Lehtomäki, I. Makkonen, M. A. Caro, A. Harju, and O. J. Lopez-Acevedo, J. Chem. Phys. **141**, 234102 (2014).
[44] J. P. Perdew, K. Burke, and M. Ernzerhof, Phys. Rev. Lett. **77**, 3865 (1996).
[45] J. P. Perdew and Y. Wang, Phys. Rev. B **45**, 13244 (1992).
[46] N. Marzari and D. Vanderbilt, Phys. Rev. B **56**, 12847 (1997).
[47] I. Souza, N. Marzari, and D. Vanderbilt, Phys. Rev. B **65**, 035109 (2001).
[48] M. P. L. Sancho, J. M. L. Sancho, J. M. L. Sancho, and J. Rubio, J. Phys. F **15**, 851 (1985).
[49] Q. S. Wu, S. N. Zhang, H. F. Song, M. Troyer, and A. A. Soluyanov, Comput. Phys. Commun. **224**, 405 (2018).
[50] I. I. Mazin, M. D. Johannes, L. Boeri, K. Koepernik, and D. J. Singh, Phys. Rev. B **78**, 085104 (2008).
[51] Z. P. Yin, S. Lebegue, M. J. Han, B. P. Neal, S. Y. Savrasov, and W. E. Pickett, Phys. Rev. Lett. **101**, 047001 (2008).
[52] W. E. Pickett, Phys. Rev. B **58**, 4335 (1998).
[53] D. J. Singh, New J. Phys. **14**, 123003 (2012).
[54] G. T. Wang, H. P. Zhang, L. Zhang, and C. Liu, J. Appl. Phys. **113**, 243904 (2013).
[55] X. W. Yan and Z. Y. Lu, J. Phys.: Condens. Matter **25**, 365501 (2013).
[56] D. V. Suetin and A. L. Ivanovskii, J. Alloys Compd. **564**, 117 (2013).
[57] D. V. Suetin and A. L. Ivanovskii, JETP Lett. **97**, 220 (2013).
[58] T. Yajima, K. Nakano, F. Takeiri, Y. Nozaki, Y. Kobayashi, and H. Kageyama, J. Phys. Soc. Jpn. **82**, 033705 (2013).
[59] Z. Zhu, G. W. Winkler, Q. S. Wu, J. Li, and A. A. Soluyanov, Phys. Rev. X **6**, 031003 (2016).

[60] X. Feng, C. M. Yue, Z. D. Song, Q. S. Wu, and B. Wen, Phys. Rev. Mater. **2**, 014202 (2017).

[61] L. M. Schoop, L. S. Xie, R. Chen, Q. D. Gibson, S. H. Lapidus, I. Kimchi, M. Hirschberger, N. Haldolaarachchige, M. N. Ali, C. A. Belvin, T. Liang, J. B. Neaton, N. P. Ong, A. Vishwanath, and R. J. Cava, Phys. Rev. B **91**, 214517 (2015).

[62] H. Leng, C. Paulsen, Y. K. Huang, and A. de Visser, Phys. Rev. B **96**, 220506(R) (2017).

[63] G. Bian, T.-R. Chang, R. Sankar, S.-Y. Xu, H. Zheng, T. Neupert, C.-K. Chiu, S.-M. Huang, G. Chang, I. Belopolski, D. S. Sanchez, M. Neupane, N. Alidoust, C. Liu, B. Wang, C.-C. Lee, H.-T. Jeng, C. Zhang, Z. Yuan, S. Jia *et al.*, Nat. Commun. **7**, 10556 (2016).